Ocean Engineering 92 (2014) 1–11

Contents lists available at ScienceDirect

Ocean Engineering

journal homepage: www.elsevier.com/locate/oceaneng

Modelling axisymmetric codends made of hexagonal mesh types

D. Priour *

French Institute of Marine Research (IFREMER), Plouzane Cedex, France

ARTICLE INFO

Article history:
Received 22 November 2013
Accepted 28 September 2014
Available online 22 October 2014

Keywords:
Codends
Hexagonal meshes
Trawl selectivity
Simulation
Twine tensions
Catch force

ABSTRACT

Codends are the rear parts of trawls, which collect the catch and where most of the selectivity process occurs. Selectivity is the process by which the large fish are retained while the small ones are released. The codends applied in many fisheries often consist of only one type of mesh. Therefore it is reasonable to consider these codends as being axisymmetric. Their shapes depend mainly on the volume of catch, on the shape of meshes (diamond, square, hexagonal) and on the number of meshes along and around the codend. The shape of the codends is of prime importance in order to understand the selectivity process. This paper presents a model of deformation of codends made up of hexagonal meshes. Two types of hexagonal meshes have been investigated: the T0 codend where two sides of the hexagons are in axial planes and the T90 codend where two sides are perpendicular to the codend axis. The forces involved in this model are twine tension and catch pressure. A Newton–Raphson scheme has been used to calculate the equilibrium.

1. Introduction

Fishing operations target the largest sized fish mostly. The catch often contains considerable amounts of undersized fish or non-targeted species. This non-target catch could reach one-third of the total marine harvest worldwide (Alverson and Hughes, 1996).

In order to reduce this wasteful bycatch, studies of trawl selectivity have been carried out at sea. But due to the large number of uncontrollable parameters, numerous trials have to be undertaken in order to reach good quality statistics. This leads to expensive studies which are often inconclusive.

To overcome this uncertainty, it is possible to use predictive models of codend selectivity. Such models (e.g. PRESEMO, Herrmann et al., 2006, 2007) have been developed in the last few years and are able to simulate codend selectivity quickly and simply. Even though these tools are based on approximations, their results are often reliable. However, it is important to know the fish behaviour and the mechanical codend behaviour.

To understand better the codend behaviour, it is essential to gather data on the mesh openness along the codend when the catch builds up. This opening also depends on the design of the codend, i.e. the mesh type (diamond, square, hexagonal), the number of meshes around and along, the size of meshes. Two numerical models developed in recent years are already able to assess codend geometries: O'Neill (1997) derives differential equations that govern the geometry of axisymmetric codends for a range of different mesh shapes, and Priour (1999, 2013) has developed a more general three-dimensional finite element method model of netting deformation. Both of these models can take into account the elasticity and flexural rigidity of the twines, the mesh shapes (diamond, square, hexagonal), and the hydrodynamic forces that act on the netting material and catch. Their numerical simulations were compared by O'Neill and Priour (2009) and were found to be very similar.

In a previous paper (Priour et al., 2009), an axisymmetric model of the codend made up of diamond, square or rectangular meshes has been developed by looking at the force balance on the twine elements on a meridian along the codend length. The advantage of this model over those above is that it is easy to implement and its solution does not depend on the use of licensed software.

The diamond mesh codend is the codend type which has traditionally been applied in many trawl fisheries. This type of codend could be modelled by numerical models such as those previously described. In recent decades there has been a tendency to use netting with thicker twine (Herrmann et al., 2013). In this case the use of an ideal diamond shape model is not perfect due to the size of the knots. As mentioned by Sistiaga et al. (2011), a hexagonal mesh model is preferable compared to a diamond mesh model to describe the actual shape of the meshes in the codends (Fig. 2). This means the knots are sides of the hexagon.

In this present paper this previous model (Priour et al., 2009) has been extended to hexagonal meshes. Two types of hexagonal meshes are investigated: the T0 type, where twines are in axial

* Tel.: +33 2 98 22 41 81; fax: +33 2 98 22 85 47.
E-mail address: daniel.priour@ifremer.fr

http://dx.doi.org/10.1016/j.oceaneng.2014.09.037
0029-8018/

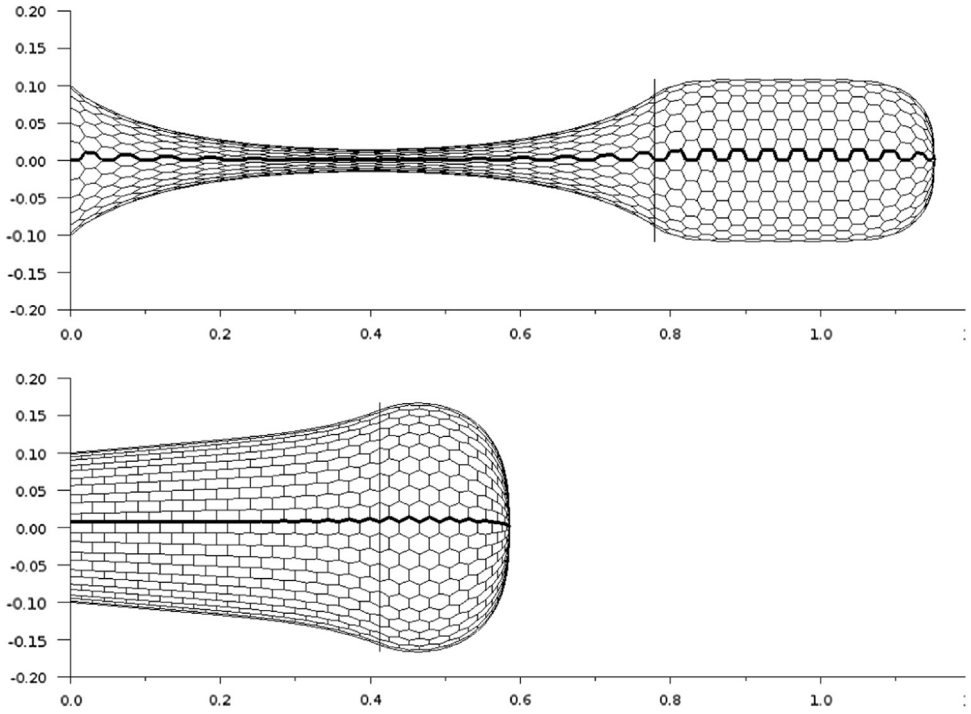

Fig. 1. The two types of hexagonal meshes investigated in the paper: the T0 at the top where some twines are in axial planes and the T90 where some twines are in planes perpendicular to the codend axis. The two codends are made up of the same piece of netting (24 by 24 meshes) and the catch covers the same number of meshes (10). The vertical line is the limit of the catch. Due to axisymmetry only one meridian is calculated (highlighted row).

planes (the angle between this axial plane and the axis of the codend is 0°) and the T90 type where twines are in planes perpendicular to the codend axis (the angle between this plane and the axis of the codend is 90°, Fig. 1). Although in most fisheries the codends are T0 type (the knots are in axial planes), in some cases, e.g. Baltic Sea for cod fishery (Anon, 2005), the codends of T90 type are legal (the knots are perpendicular to the codend axis).

This model is supposed to represent usual netting where the knots are large enough to consider their size as one side of the hexagonal mesh. Obviously the six sides of the hexagon are not necessarily equal (Fig. 2).

2. The T0 codend

By assuming axisymmetry, the codend geometry can be determined by examining the nodes belonging to one row of twine along the codend length. This row is highlighted at the top of Fig. 1 and in Fig. 3. This row is called the meridian. The approach consists of three steps. Firstly, the initial position of these nodes, consistent with the boundary conditions, must be defined. Then, the forces acting on these nodes are calculated. Finally, using the Newton–Raphson method (Priour, 2013), the equilibrium position of these nodes is evaluated.

The forces that act on the codend are the twine tensions and the hydrodynamic forces. As shown by O'Neill and O'Donoghue (1997), the hydrodynamic forces that act on the unblocked netting are negligible in comparison with the pressure forces acting on the netting where the catch blocks the meshes. Consequently, it is only necessary to consider the twine tensions and the pressure forces that act in the region of the catch.

2.1. Nodes of the T0 codend

The meridian is such that some nodes of this meridian are in the plane *XOZ*, as shown in Fig. 3. The mesh *i* (trapeze in Fig. 3) is made up of 6 twines and 4 nodes (*ia*, *ib*, *ic* and *id*). The nodes *ja*, *jb*, *jc* and *jd* belong to the same mesh ring but they do not belong to the calculated meridian (highlighted meridian in Fig. 3). In Fig. 3 the node $i-1d$ belongs to the previous mesh $(i-1)$ and the node $i+1a$ belongs to the following mesh $(i+1)$. The nodes of the calculated meridian with suffixes *a* and *d* (e.g. *ia*, *id*, $i-1d$, $i+1a$) belong to the plane *XOZ* (their *y* coordinates are 0 as shown in Fig. 3). The nodes of the calculated meridian with suffixes *b* and *c* (e.g. *ib*, *ic*, $i-1b$, $i+1c$) do not belong to the plane *XOZ*, they are in a radial plane which gives an angle θ with the plane *XOZ*. With

$$\theta = \frac{\pi}{nbr} \tag{1}$$

where θ is the angle between the two radial planes passing by *ia* and *ib* (*Rad*) and *nbr* is the number of meshes around.

The reason is that the neighbouring nodes *ja* and *jd* belong to a radial plane which gives an angle 2θ with the plane *XOZ*. This is due to axisymmetry. Likewise the nodes *jb* and *jc* belong to another radial plane which gives an angle -2θ with the plane *XOZ*. Due to equilibrium, the nodes *ib* and *ic* have to be in a radial plane just between the radial planes of *ja* and *ia*.

From this definition of node positions, we are able to say

$$ia = (ia_x, 0, ia_r)$$

With ia_x the position of *ia* along the *X*-axis and ia_r its radial position,

$$ib = (ib_x, ib_r \sin\theta, ib_r \cos\theta)$$
$$ic = (ic_x, ic_r \sin\theta, ic_r \cos\theta)$$
$$id = (id_x, 0, id_r)$$

where suffix $_x$ refers to the position along the *X*-axis and suffix $_r$ to the radial position.

The position of the neighbouring nodes is

$$ja = (ia_x, ia_r \sin 2\theta, ia_r \cos 2\theta)$$
$$jb = (ib_x, -ib_r \sin\theta, ib_r \cos\theta)$$

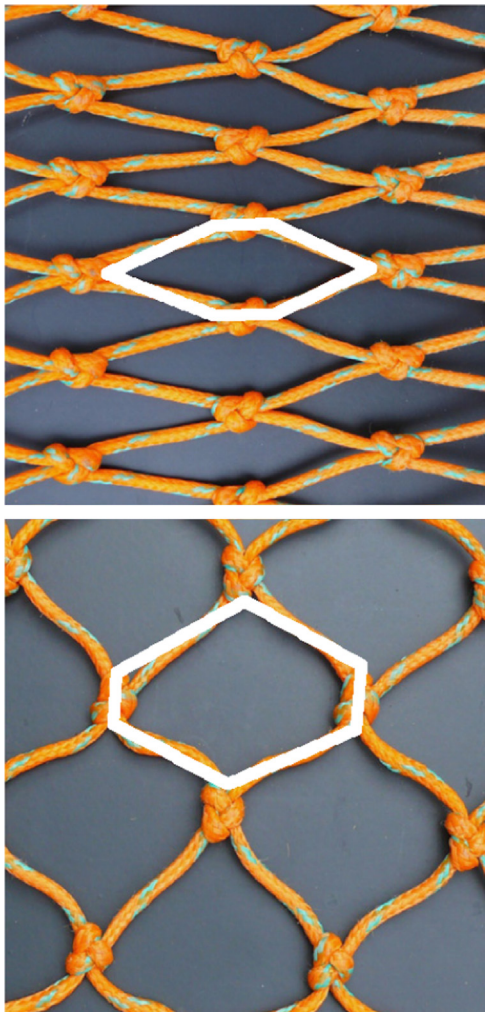

Fig. 2. Usual netting used at sea (Wienbeck et al., 2011). The meshes could be considered as hexagonal: the knot is a side of the hexagon, as highlighted. If the codend axis is horizontal, at the top the netting is of the T0 type, while at the bottom it is that of the T90.

$$jc = (ic_x, -ic_r \sin\theta, ic_r \cos\theta)$$

$$jd = (id_x, id_r \sin 2\theta, id_r \cos 2\theta)$$

It can be seen from the previous equations that the position of nodes on the meridian and of the neighbours depend only on the axial and radial positions of the nodes of the meridian (such as ia_x, ia_r, ib_x, ib_r).

2.2. Twines of the T0 codend

The twines can be defined from the node positions. A twine links 2 nodes and it is defined as a vector. 3 twine vectors emerge from each node of the meridian of mesh i: one in a plane along the axis, one going up and one going down. For example for node ib the twine between ib and ic is in the plane along the axis and it is called **Aib** (Fig. 3), **A** standing for axial. The twine between ib and ia is **Dib**, with **D** standing for downward. Finally the twine between ib and ja is **Uib**, with **U** standing for upward.

With this definition, the vectors along the twines which emerge from node ia are:

$$\mathbf{Aia} = \begin{pmatrix} i-1d_x - ia_x \\ 0 \\ i-1d_r - ia_r \end{pmatrix}, \quad \mathbf{Uia} = \begin{pmatrix} ib_x - ia_x \\ ib_r \sin\theta \\ ib_r \cos\theta - ia_r \end{pmatrix},$$

$$\mathbf{Dia} = \begin{pmatrix} ib_x - ia_x \\ -ib_r \sin\theta \\ ib_r \cos\theta - ia_r \end{pmatrix}$$

The vectors along the twines which emerge from node ib are

$$\mathbf{Aib} = \begin{pmatrix} ic_x - ib_x \\ ic_r \sin\theta - ib_r \sin\theta \\ ic_r \cos\theta - ib_r \cos\theta \end{pmatrix}, \quad \mathbf{Uib} = \begin{pmatrix} ia_x - ib_x \\ ia_r \sin 2\theta - ib_r \sin\theta \\ ia_r \cos 2\theta - ib_r \cos\theta \end{pmatrix},$$

$$\mathbf{Dib} = \begin{pmatrix} ia_x - ib_x \\ -ib_r \sin\theta \\ ia_r - ib_r \cos\theta \end{pmatrix}$$

The vectors along the twines which emerge from node ic are

$$\mathbf{Aic} = \begin{pmatrix} ib_x - ic_x \\ ib_r \sin\theta - ic_r \sin\theta \\ ib_r \cos\theta - ic_r \cos\theta \end{pmatrix}, \quad \mathbf{Uic} = \begin{pmatrix} id_x - ic_x \\ id_r \sin 2\theta - ic_r \sin\theta \\ id_r \cos 2\theta - ic_r \cos\theta \end{pmatrix},$$

$$\mathbf{Dic} = \begin{pmatrix} id_x - ic_x \\ -ic_r \sin\theta \\ id_r - ic_r \cos\theta \end{pmatrix}$$

The vectors along the twines which emerge from node id are

$$\mathbf{Aid} = \begin{pmatrix} i+1a_x - id_x \\ 0 \\ i+1a_r - id_r \end{pmatrix}, \quad \mathbf{Uid} = \begin{pmatrix} ic_x - id_x \\ ic_r \sin\theta \\ ic_r \cos\theta - id_r \end{pmatrix},$$

$$\mathbf{Did} = \begin{pmatrix} ic_x - id_x \\ -ic_r \sin\theta \\ ic_r \cos\theta - id_r \end{pmatrix}$$

Some of these twine vectors are equal:

$$\mathbf{Uia} = -\mathbf{Dib}$$
$$\mathbf{Aib} = -\mathbf{Aic}$$
$$\mathbf{Dic} = -\mathbf{Uid}$$

2.3. Twine tensions on the T0 codend

With the hypothesis of elastic twines, the force vector coming from twine tension for the twine vector **Aia** is

$$\mathbf{TAia} = \frac{|\mathbf{Aia}| - l0}{l0} EA \frac{\mathbf{Aia}}{|\mathbf{Aia}|}$$

with l_0 (m) being the un-stretched length of the twine and EA (N) the rigidity of the twine. When the twine is compressed, the rigidity is null in order to take into account the very low resistance of the twine to the compression.

The other twine tensions have similar expression.

The force on node ia coming from the twine tension is

$$\mathbf{Fia} = \mathbf{TAia} + \mathbf{TUia} + \mathbf{TDia} \tag{2}$$

From the other 3 nodes (ib, ic and id) of the mesh i, the forces have similar expression.

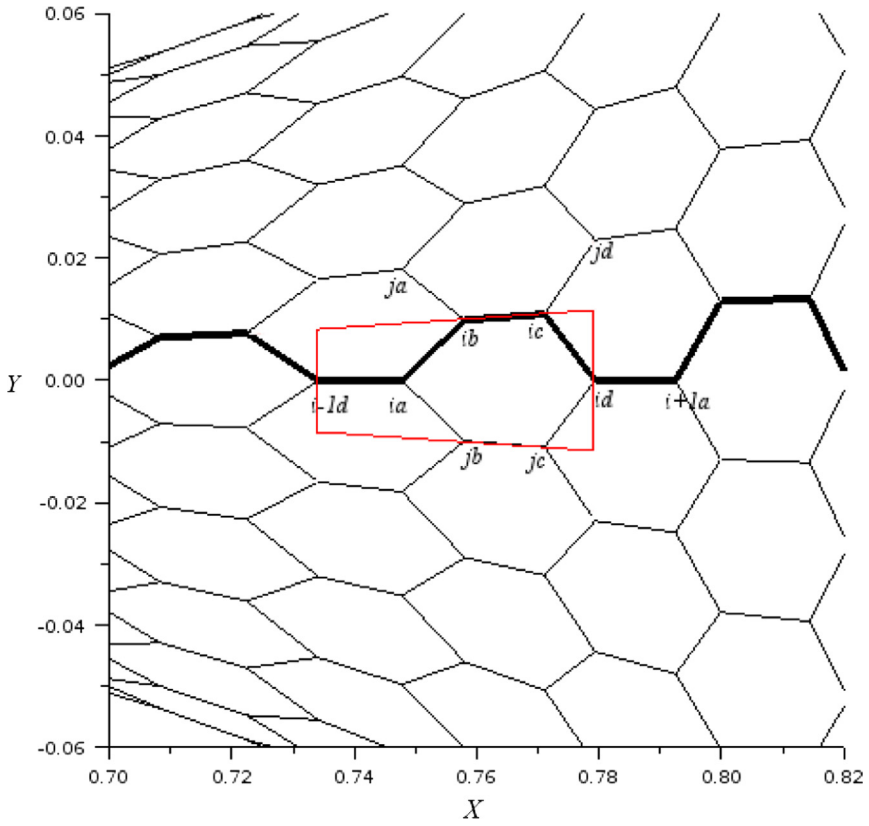

Fig. 3. Definition of nodes of the T0 codend. Two nodes of the mesh *i* belong to the plane *XOZ* (*ia* and *id*) and two nodes belong to another radial plane (*ib* and *ic*). The neighbours are *ja*, *jb*, *jc* and *jd*. The trapeze represents one mesh.

2.4. Catch pressure

The hydrodynamic forces that act on the catch exert a pressure force on the codend netting that can be described by Priour (2013)

$$P=\frac{1}{2}\rho C_d V^2 \tag{3}$$

where P is the pressure due to the catch (N/m^2), ρ is the water density (1025 kg/m^3), C_d is the drag coefficient on the catch (C_d=1.4, Priour, 2013), and V is the towing speed (m/s).

For the T0 codend with a catch which covers the nodes *ia* and *ib*, the surface involved by the pressure of the catch for these two nodes is defined by the trapeze in Fig. 4. This trapeze is in fact a part of a cone. This surface is limited along the *X*-axis by the nodes *ia* and *ib* and it is limited around by an angle of $2\pi/nbr$ or 2θ as defined in Eq. (1). This part of the cone is limited by 2 circles of radius ia_r and ib_r. This means that the axial surface of this part of the cone is

$$\theta|ia_r^2-ib_r^2|$$

This part of the cone is also visible in Fig. 5. Due to the inclination of the cone the radial surface involved is

$$\theta(ia_x-ib_x)(ia_r+ib_r)$$

Once the axial and radial surfaces are determined, the forces on the nodes *ia* and *ib* due to the effect of the pressure of the catch on this part of the cone (cf. Figs. 4 and 5) are

$$Fa_x=\theta|ia_r^2-ib_r^2|\frac{P}{2} \tag{4}$$

$$Fb_x=\theta|ia_r^2-ib_r^2|\frac{P}{2} \tag{5}$$

$$Fa_r=\theta(ia_x-ib_x)(ia_r+ib_r)\frac{P}{2} \tag{6}$$

$$Fb_r=\theta(ia_x-ib_x)(ia_r+ib_r)\frac{P}{2} \tag{7}$$

with Fa_x (Fb_x) being the force on the node *ia* (*ib*) along the *X*-axis and Fa_r (Fb_r) the force on the node *ia* (*ib*) along the radial. These forces are due to the portion of netting between nodes *ia* and *ib*. In the same way, if the catch covers the netting between nodes *ib* and *ic* the forces due to the pressure of the catch are

$$Fb_x=\theta|ib_r^2-ic_r^2|\frac{P}{2} \tag{8}$$

$$Fc_x=\theta|ib_r^2-ic_r^2|\frac{P}{2} \tag{9}$$

$$Fb_r=\theta(ib_x-ic_x)(ib_r+ic_r)\frac{P}{2} \tag{10}$$

$$Fc_r=\theta(ib_x-ic_x)(ib_r+ic_r)\frac{P}{2} \tag{11}$$

2.5. Positions and forces in the T0 codend

It has been seen previously that the unknowns of these equations are only ia_x, ia_r, ib_x, ib_r, ic_x, ic_r, id_x and id_r for the mesh *i*. This means that the total unknowns for the whole meridian are

$$\mathbf{X}=(0d_x, 0d_r, 1a_x, 1a_r, \ldots, ia_x, ia_r, ib_x, ib_r, ic_x, ic_r, id_x, id_r, \ldots, nd_x, nd_r)$$

This vector of polar positions begins by the node 0*d* which begins mesh 1 and it is followed by the four nodes of mesh 1 (1*a*, 1*b*, 1*c* and 1*d*) and finishes with the four nodes of the last mesh *n* (*na*, *nb*, *nc* and *nd*). In order to use the Newton–Raphson method to find the equilibrium position of the meridian, the force vector **F**

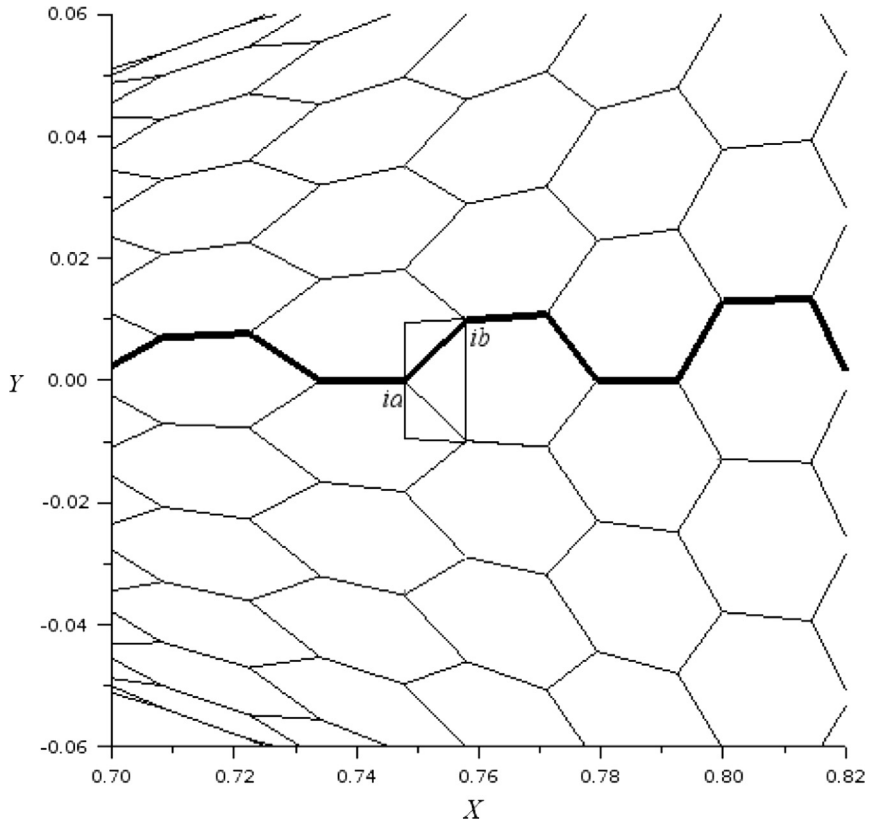

Fig. 4. T0 codend. The trapeze defines the surface of netting involved by the catch for the nodes (*ia* and *ib*).

must follow the same order:

$$\mathbf{F}=\begin{pmatrix} F0d_x \\ F0d_r \\ F1a_x \\ F1a_r \\ . \\ Fia_x \\ Fia_r \\ Fib_x \\ Fib_r \\ Fic_x \\ Fic_r \\ Fid_x \\ Fid_r \\ . \\ Fnd_x \\ Fnd_r \end{pmatrix}$$

This means that for each node the polar components of force (Fia_x and Fia_r for node i) have to be calculated from Cartesian components (Fia_x, Fia_y and Fia_z of Eq. (2)) and from the forces already known (Eqs. (4)–(11)).

For nodes of types *a* and *d* the polar components of forces are

$$Fia_x = Fia_x$$
$$Fia_r = Fia_z$$
$$Fid_x = Fid_x$$
$$Fid_r = Fid_z$$

because these nodes are in the plane *XOZ* and consequently the *z* coordinate is also the *r* coordinate.

For the nodes of types *b* and *c* the polar components of forces are

$$Fib_x = Fib_x$$
$$Fib_r = \sin\ \theta Fib_y + \cos\ \theta Fib_z$$
$$Fic_x = Fic_x$$
$$Fic_r = \sin\ \theta Fic_y + \cos\ \theta Fic_z$$

because these nodes are in a radial plane which gives an angle θ with the plane *XOZ*.

With these conditions the force vector is

$$\mathbf{F}=\begin{pmatrix} F0d_x \\ F0d_z \\ F1a_x \\ F1a_z \\ . \\ Fia_x \\ Fia_z \\ Fib_x \\ \sin\ \theta Fib_y + \cos\ \theta Fib_z \\ Fic_x \\ \sin\ \theta Fic_y + \cos\ \theta Fic_z \\ Fid_x \\ Fid_z \\ . \\ Fnd_x \\ Fnd_z \end{pmatrix}$$

2.6. Boundary conditions of the T0 codend

The boundary conditions of the model have to be determined. They are the entrance and closure of the codend. At the entrance the radius is given and fixed and at the closure the radius must be 0 m. This means that for the vector position of the nodes, **X** is such that

$$0d_x = 0$$
$$0d_r = r_0$$
$$nd_r = 0$$

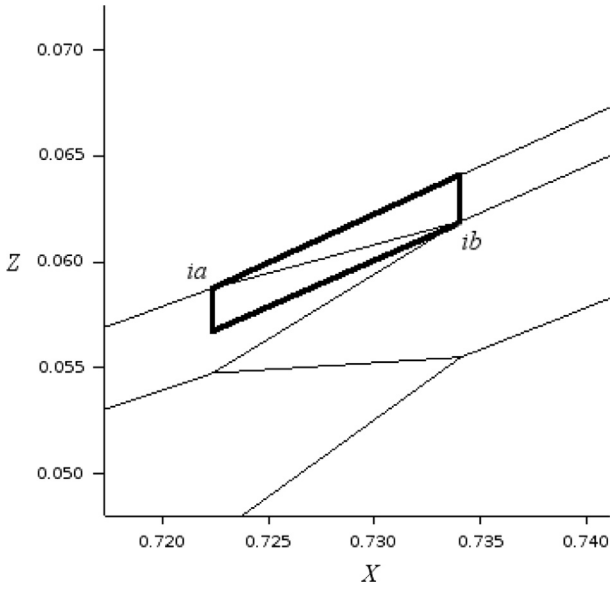

Fig. 5. Side view of the T0 codend. The trapeze defines the surface of netting involved by the catch for the nodes (*ia* and *ib*).

The node 0*d* refers to the entrance and the node *nd* refers to the closure. r_0 is the entrance radius.

2.7. Newton–Raphson solver

The force components are added at each node in the vector **F** and the Newton–Raphson scheme is used to assess the equilibrium position. This method is an iterative method where, for each iteration k, the displacement of the nodes $\mathbf{h}_k$ is calculated by the equation

$$\mathbf{h}_k = \frac{\mathbf{F}(\mathbf{X}_k)}{-F'(\mathbf{X}_k)}$$

where $\mathbf{h}_k$ is the displacement vector of the nodes (m), $\mathbf{F}(\mathbf{X}_k)$ is the force vector on the nodes (N), and $-F'(\mathbf{X}_k)$ is the stiffness matrix calculated as the derivative of **F** relative to $\mathbf{X}(N/m)$.

The position at the next iteration $\mathbf{X}_{k+1}$ is then calculated by $\mathbf{X}_{k+1} = \mathbf{X}_k + \mathbf{h}_k$. This process is repeated until the residual force, $\mathbf{F}(\mathbf{X})$, is less than a predefined amount.

It is necessary to determine an initial position of the nodes along the codend, which is assumed at this point to be a straight horizontal line aligned at the entrance radius except for the last node which is on the axis of the codend closure. Thus, the initial shape of the codend is a cylinder.

2.8. Results

Fig. 1 at the top is the result of this model. The conditions of this calculation are

- $n = 24$, number of meshes along;
- $nbp = 10$, number of meshes affected by the catch;
- $nbr = 24$, number of meshes around;
- $l_0 = 0.015$ m, length of un-stretched twines in the axial plane;

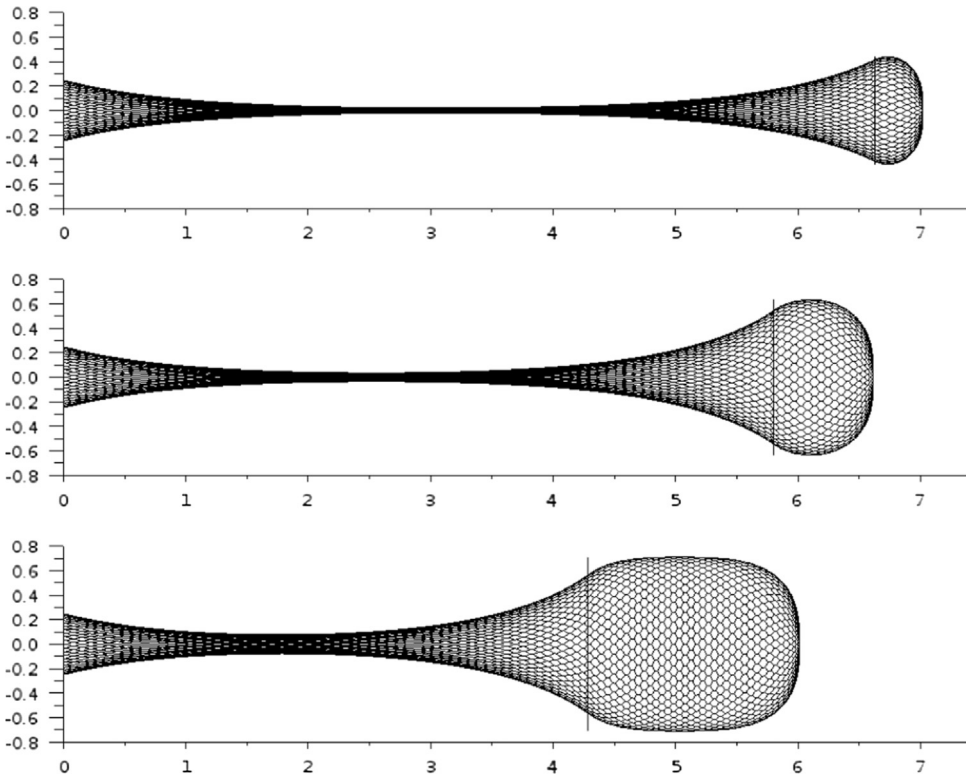

Fig. 6. T0 codend made of usual netting shown in Fig. 2. The netting is 50 by 50 meshes. The knot is 2.5 cm long when the twine is 5 cm long. The catch covers 5 meshes at the top, 10 in the middle and 20 at the bottom. This figure must be compared to Fig. 9, where the same piece of netting is used but turned 90°.

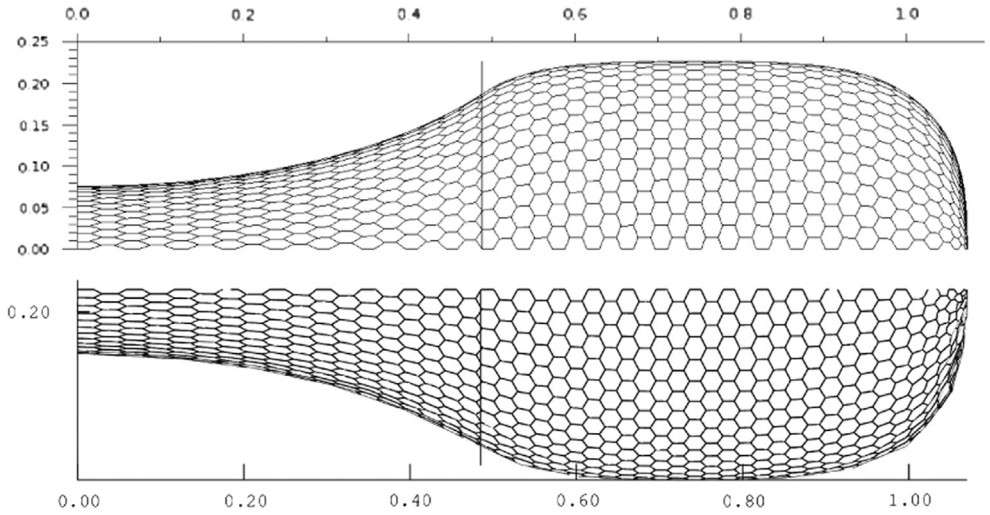

Fig. 7. The top figure is from the present model and the bottom is from a 3D one. The shapes are pretty similar.

- $m_0 = 0.015$ m, length of un-stretched twines out of the axial plane;
- $EA = 450$ N/m, stiffness of twines;
- $V = 1.0$ m/s, towing speed;
- $r_0 = 0.1$ m, entrance radius.

To clarify the difference between l_0 and m_0 it is pointed out that at the top of Fig. 2, l_0 refers to the length of knots while m_0 refers to the length of twines.

In the following example of Fig. 6 a netting which attempts to represent the netting of Fig. 2 has been used.

In this case

- $n = 50$, number of meshes along;
- $nbp = 5, 10, 20$, number of meshes affected by the catch;
- $nbr = 50$, number of meshes around;
- $l_0 = 0.025$ m, length of un-stretched twines in the axial plane (knot);
- $m_0 = 0.050$ m, length of un-stretched twines out of the axial plane (twine);
- $EA = 68{,}000$ N/m, stiffness of twines;
- $V = 1.5$ m/s, towing speed;
- $r_0 = 0.25$ m, entrance radius.

The calculation also finds for a catch covering 10 meshes:

- The traction on entrance = 1507.53 N.
- The drag on the catch = 1507.54 N.
- The maximal radius = 0.636 m.
- The thickness of the catch = 0.818 m.
- The length of the codend = 6.616 m.
- The surface of the netting in contact with the catch = 3.592 m^2.
- The volume inside the netting in contact with the catch = 0.832 m^3.

It can be seen that, as expected, the reaction on the entrance equals the drag on the catch. This equality can be explained by mechanical considerations: the external forces involved in the model are only the reaction at the entrance and the drag on the catch. Due to equilibrium, the sum of these two forces must be null, in other words, their amplitude must be equal.

2.9. Verification with the 3D model

In a previous study (Priour, 2003) we developed a 3D model for hexagonal mesh netting. A comparison has been made between these two models.

In the present model and in the 3D model (Priour, 2003) the conditions are identical and are

- $n = 25$, number of meshes along;
- $nbp = 16$, number of meshes affected by the catch;
- $nbr = 50$, number of meshes around;
- $l_0 = 0.015$ m, length of un-stretched twines in the axial plane;
- $m_0 = 0.015$ m, length of un-stretched twines out of the axial plane
- $EA = 450$ N/m, stiffness of twines;
- $V = 1.0$ m/s, towing speed;
- $r_0 = 0.20$ m, entrance radius.

Fig. 7 shows a graphic comparison between the two shapes.
The calculation also finds

- The traction on entrance is 79.1 N for the present model and 76.8 N for the 3D model.
- The maximal radius is 0.227 m for the present model and 0.227 m for the 3D model.
- The thickness of the catch is 0.585 m for the present model and 0.585 m for the 3D model.

The two models are in pretty good accordance.

2.10. Verification with the maximal diameter of the diamond codend

In the case of the codend made up of diamond meshes and which is completely full and long enough, there is an analytical value for the maximal diameter of the codend (O'Neill and Priour, 2009):

$$R_{max} = \frac{2nbrl_0}{\pi\sqrt{6}}$$

In the case of the diamond codend with

- $n = 30$, number of meshes along;
- $nbp = 30$, number of meshes affected by the catch;
- $nbr = 30$, number of meshes around;
- $m_0 = 0.04$ m, length of twines.

The maximal radius is $R_{max} = 0.3119$ m.

To model this codend with the present model, the length of the twine along the axial plane has been reduced to a very small value 0.000004 m. This gives the present T0 model in the following conditions:

- $n = 30$, number of meshes along;
- $nbp = 30$, number of meshes affected by the catch;
- $nbr = 30$, number of meshes around;
- $l_0 = 0.000004$ m, length of un-stretched twines in the axial plane;
- $m_0 = 0.04$ m, length of un-stretched twines out of the axial plane;
- $EA = 68{,}000$ N/m, stiffness of twines;
- $V = 1.0$ m/s, towing speed;
- $r_0 = 0.25$ m, entrance radius.

The present model gives a maximal radius of $R_{max} = 0.311908$ m. This value is very close to the expected one (0.3119 m).

3. The T90 codend

By assuming axisymmetry, the codend geometry can be determined by examining the nodes belonging to one row of twine along the codend length. This row is highlighted at the bottom of Fig. 1 and in Fig. 8 and it is called the meridian.

As mentioned previously (Section 2), it is only necessary to consider the twine tensions and the pressure forces that act in the region of the catch.

3.1. Nodes of the T90 codend

The meridian consists of nodes from $i1$ to im. The node $i1$ is at the entrance while im is the last node. The row of nodes from $j1$ to jm is just above the meridian in Fig. 8, while the row of nodes from $k1$ to km is just below the meridian. Consequently the distance between nodes $j4$ and $k4$ covers just one mesh around. This is true for nodes j and k with the same suffix (4, 5 …).

A mesh around covers an angle θ which is

$$\theta = \frac{2\pi}{nbr} \tag{12}$$

where nbr is the number of meshes around.

The nodes j with an odd suffix ($j5$, $j7$ …) are not noted in Fig. 8, because they are not used in the following. The plane XOZ is chosen in order to be in the middle of the nodes i and k.

This means that if

$$i4 = (i4_x, i4_y, i4_z)$$
$$k4 = (i4_x, -i4_y, i4_z)$$

Consequently the angle between node $k4$ and the plane XOZ is such that

$$\tan\ \beta 4 = \frac{i4y}{i4z}$$

It follows that the angle between the plane XOZ and the node $j4$ is $\theta - \beta 4$.

This gives for node $j4$:

$$j4 = (i4_x, i4_r\ \sin(\theta - \beta 4), i4_r\ \cos(\theta - \beta 4))$$

With $i4_r$ the radius of node $i4$:

$$i4_r = \sqrt{i4_y^2 + i4_z^2}$$

Accordingly, once the Cartesian coordinates of node $i4$ are known the coordinates of $k4$ and $j4$ are also known. This is true whatever the suffix of node i.

If the number of meshes along is n, the suffix of the last node m is

$$m = 2n + 1$$

3.2. Twines of the T90 codend

The twines can be defined from node positions. A twine links 2 nodes and it is defined as a vector.

Three twine vectors emerge from each node of the meridian: one around the codend, one backward and one forward. For

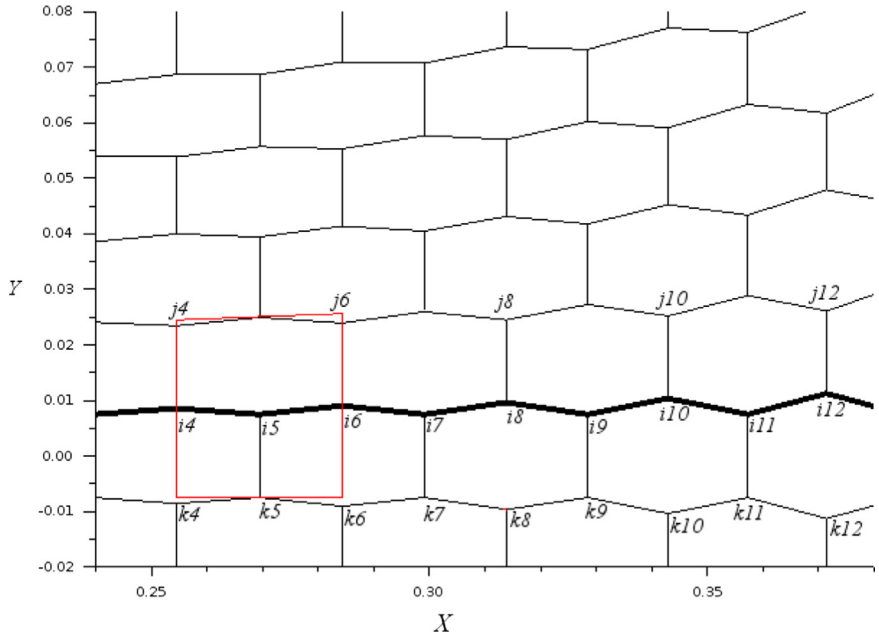

Fig. 8. Definition of nodes of the T90 codend. The nodes along the meridian are $i1$ to im. The top neighbours are $j1$ to jn while the bottom neighbours are $k1$ to km. Nodes k are symmetric to i in relation to the plane XOZ and the nodes j to k cover 1 mesh around. The trapeze represents one mesh.

example for node $i5$, the twine between $i5$ and $i4$ is backward and it is called **Bi5** (Fig. 8), **B** for backward. The twine between $i5$ and $i6$ is **Fi5**, with **F** for forward. Finally the twine between $i5$ and $k5$ is **Ai5**, with **A** for around.

According to this definition, the vectors along the twines which emerge from node $i4$ are

$$\mathbf{Bi4}=\begin{pmatrix} i3_x-i4_x \\ i3_y-i4_y \\ i3_z-i4_z \end{pmatrix},\quad \mathbf{Fi4}=\begin{pmatrix} i5_x-i4_x \\ i5_y-i4_y \\ i5_z-i4_z \end{pmatrix},\quad \mathbf{Ai4}=\begin{pmatrix} j4_x-i4_x \\ j4_y-i4_y \\ j4_z-i4_z \end{pmatrix}$$

According to this definition, the vectors along the twines which emerge from node $i5$ are

$$\mathbf{Bi5}=\begin{pmatrix} i3_x-i5_x \\ i3_y-i5_y \\ i3_z-i5_z \end{pmatrix},\quad \mathbf{Fi5}=\begin{pmatrix} i5_x-i5_x \\ i5_y-i5_y \\ i5_z-i5_z \end{pmatrix},\quad \mathbf{Ai5}=\begin{pmatrix} k5_x-i5_x \\ k5_y-i5_y \\ k5_z-i5_z \end{pmatrix}$$

Some of these twine vectors are equal:

$$\mathbf{Bi4}=-\mathbf{Fi3}$$
$$\mathbf{Bi5}=-\mathbf{Fi4}$$
$$\mathbf{Bi6}=-\mathbf{Fi5}$$

3.3. Twine tensions on the T90 codend

Following the same scheme of Section 2.3, the force vectors coming from twine tension are calculated and consequently the forces on nodes. For example in the case of the twine vector **Ai4**, the force vector is

$$\mathbf{TAi4}=\frac{|\mathbf{Ai4}|-l0}{l0}EA\frac{\mathbf{Ai4}}{|\mathbf{Ai4}|}$$

and the force on node $i4$ is

$$\mathbf{Fi4}=\mathbf{TAi4}+\mathbf{TBi4}+\mathbf{TFi4} \tag{13}$$

3.4. Catch pressure

In the case of the T90 codend and of a catch which covers the portion of netting between nodes $i4$ and $i5$, as seen previously (Section 2.4)

$$Fi4_x=\theta|i4_r^2-i5_r^2|\frac{P}{2}$$
$$Fi5_x=\theta|i4_r^2-i5_r^2|\frac{P}{2}$$
$$Fi4_r=\theta(i4_x-i5_x)(i4_r+i5_r)\frac{P}{2}$$
$$Fi5_r=\theta(i4_x-i5_x)(i4_r+i5_r)\frac{P}{2} \tag{14}$$

with $Fi4_x$ ($Fi5_x$) being the force on node $i4$ ($i5$) along the X-axis, $Fi4_r$ ($Fi5_r$) the force on node $i4$ ($i5$) along the radial and P determined by Eq. (3). These forces are due to the portion of netting between nodes $i4$ and $i5$. In the same way, if the catch covers the netting between nodes $i5$ and $i6$, the forces due to the pressure of the catch are

$$Fi5_x=\theta|i5_r^2-i6_r^2|\frac{P}{2}$$
$$Fi6_x=\theta|i5_r^2-i6_r^2|\frac{P}{2}$$
$$Fi5_r=\theta(i5_x-i6_x)(i5_r+i6_r)\frac{P}{2}$$
$$Fi6_r=\theta(i5_x-i6_x)(i5_r+i6_r)\frac{P}{2}$$

From these radial forces ($Fi4_r$) it is necessary to calculate the Cartesian force components ($Fi4_y$ and $Fi4_z$) as it has been done for forces due to twine tension. Since the angle $\beta 4$ is already known

$$Fi4y=Fi4r\ \sin\ \beta 4 \tag{15}$$

$$Fi4z=Fi4r\ \cos\ \beta 4 \tag{16}$$

and

$$Fi5y=Fi5r\ \sin\ \beta 5$$
$$Fi5z=Fi5r\ \cos\ \beta 5$$

3.5. Positions and forces in the T90 codend

It has been seen previously that the unknowns of these equations are only the Cartesian coordinates of the nodes along the meridian ($i4_x$, $i4_y$, $i4_z$, $i5_x$, $i5_y$, $i5_z$…). This means that the total unknowns for the whole meridian are

$$\mathbf{X}=(i1_x,i1_y,i1_z,\ldots,i4_x,i4_y,i4_z,\ldots,in_x,in_y,in_z)$$

This vector of Cartesian positions begins with the node at the entrance ($i1_x$, $i1_y$ and $i1_z$) and finishes with the node on the cod-line ($n1_x$, $n1_y$ and $n1_z$). In order to use the Newton–Raphson method for finding the equilibrium position of the meridian, the force vector **F** must have the same order:

$$\mathbf{F}=\begin{pmatrix} F1_x \\ F1_y \\ F1_z \\ . \\ F4_x \\ F4_y \\ F4_z \\ . \\ Fn_x \\ Fn_y \\ Fn_z \end{pmatrix}$$

This means that for each node the Cartesian components of force ($F4_x$, $F4_y$ and $Fi4_z$ for node $i4$) have to be calculated from Cartesian components ($i4_x$, $i4_y$ and $i4_z$) already known (Eqs. (13)–(16)).

3.6. Boundary conditions of the T90 codend

The boundary conditions of the model have to be determined. They are the entrance and closure of the codend. At the entrance the radius is given and fixed (to r_0) and at the closure the radius must be 0 m:

$$i1_x=0$$
$$i1_r=r_0$$
$$nd_r=0$$

If we accept that the length between $i1$ to $k1$ is only l_0

$$i1_y=\frac{l_0}{2}$$
$$i1_z=\sqrt{r_0^2-\left(\frac{l_0}{2}\right)^2}$$

3.7. Newton–Raphson solver

The force components are added at each node in vector **F** and the Newton–Raphson scheme is used to assess the equilibrium position. This method is an iterative method where, for each iteration k, the displacement of the nodes $\mathbf{h}_k$ is calculated by the

equation

$$\mathbf{h}_k = \frac{\mathbf{F}(\mathbf{X}_k)}{-F'(\mathbf{X}_k)}$$

where $\mathbf{h}_k$ is the displacement vector of the nodes (m), $\mathbf{F}(\mathbf{X}_k)$ is the force vector on the nodes (N), and $-F'(\mathbf{X}_k)$ is the stiffness matrix calculated as the derivative of $\mathbf{F}$ relative to $\mathbf{X}$ (N/m).

The position at the next iteration $\mathbf{X}_{k+1}$ is then calculated by $\mathbf{X}_{k+1} = \mathbf{X}_k + \mathbf{h}_k$. This process is repeated until the residual force, $\mathbf{F}(\mathbf{X})$, is less than a predefined amount.

It is necessary to determine an initial position of the nodes along the codend, which is assumed at this point to be a straight horizontal line aligned on the entrance radius except for the last node which is on the axis for the closure of the codend. Thus, the initial shape of the codend is a cylinder.

3.8. Results

Fig. 1 at the bottom is the result of this model. The conditions of this calculation are

- $n = 24$, number of meshes along;
- $nbp = 10$, number of meshes affected by the catch;
- $nbr = 24$, number of meshes around;
- $l_0 = 0.015$ m, length of un-stretched twines normal to the axial plane;
- $m_0 = 0.015$ m, length of un-stretched twines out of the axial plane;
- $EA = 450$ N/m, stiffness of twines;
- $V = 1.0$ m/s, towing speed;
- $r_0 = 0.1$ m, entrance radius.

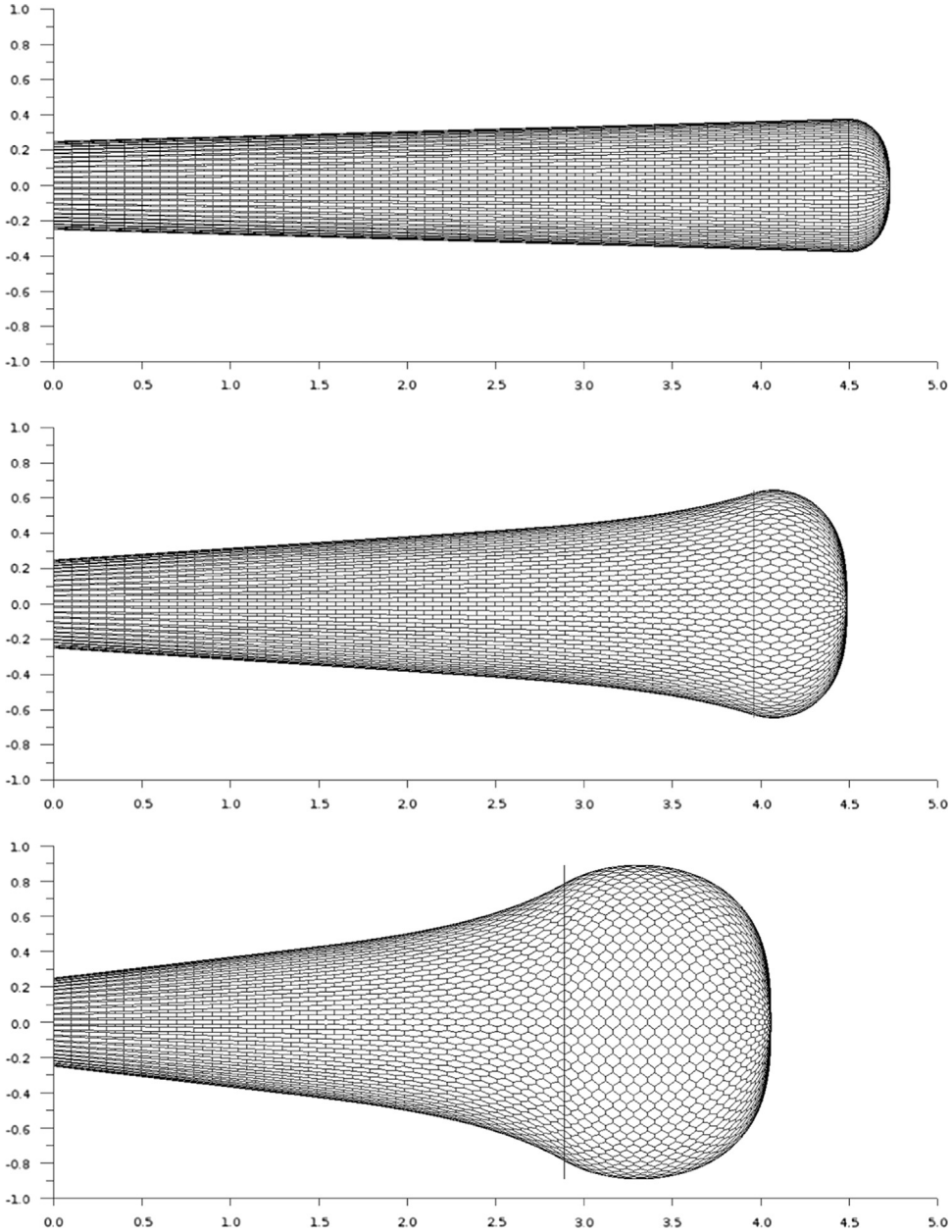

Fig. 9. T90 codend made up of the usual netting shown in Fig. 2. The netting is 50 by 50 meshes. The knot is 2.5 cm long when the twine is 5 cm long. The catch covers 5 meshes at the top, 10 in the middle and 20 at the bottom. This figure must be compared to Fig. 6, where the same piece of netting is used but it has been turned to 90°.

To clarify the difference between l_0 and m_0 it is pointed out that at the bottom of Fig. 2, l_0 refers to the length of knots while m_0 refers to the length of twines.

In Fig. 9, a netting which attempts to represent the netting of Fig. 2 has been used.

In this case

- $n=50$, number of meshes along;
- $nbp=5$, 10, 20, number of meshes affected by the catch;
- $nbr=50$, number of meshes around;
- $l_0=0.025$ m, length of un-stretched twines normal to the axial plane (knot);
- $m_0=0.050$ m, length of un-stretched twines out of the axial plane (twine);
- $EA=68{,}000$ N/m, stiffness of twines;
- $V=1.5$ m/s, towing speed;
- $r_0=0.25$ m, entrance radius.

The calculation also finds for a catch covering 10 meshes:

- The traction on entrance = 2009.77 N.
- The drag on the catch = 2009.77 N.
- The maximal radius = 0.646 m.
- The thickness of the catch = 0.528 m.
- The length of the codend = 4.489 m.
- The surface of the netting in contact with the catch = 2.597 m^2.
- The volume inside the netting in contact with the catch = 0.542 m^3.

As expected and explained previously (Section 2.8) the reaction at the entrance equals the drag on the catch.

3.9. *Verification with the maximal diameter of the diamond codend*

To model the full codend described in Section 2.10 with the present model, the length of the twine normal to the axial plane has been reduced to a very small value 0.000004 m. This gives for the present T90 model the following conditions:

- $n=30$, number of meshes along;
- $nbp=30$, number of meshes affected by the catch;
- $nbr=30$, number of meshes around;
- $l_0=0.000004$ m, length of un-stretched twines normal to the axial plane;
- $m_0=0.04$ m, length of un-stretched twines out of the axial plane;
- $EA=68{,}000$ N/m, stiffness of twines;
- $V=1.0$ m/s, towing speed;
- $r_0=0.25$ m, entrance radius.

The present model gives a maximal radius of $R_{max}=0.311947$ m. This value is very close to the expected one (0.3119 m).

4. Discussion and conclusion

A model of codends made up of hexagonal meshes has been developed. This model is based on the approximation that the cod-ends are axisymmetric and that the twines are elastic. This model is not a complex 3D model as developed by Priour (2013) and does not depend on a licensed software as used by O'Neill (1997).

The comparison of results obtained by this model with an analytical solution or a 3D model is relatively good: the difference is less than 1% for the dimension and less than 3% on the drag.

The hypothesis that twines are fully compressible, which means that they have no resistance when compressed has been used. This hypothesis is probably debatable in the case of an usual netting where some twines are quite large, especially the knot. This point could be solved by letting the user decide about the compressibility of the twines.

The drag on the netting has not been taken into account because, generally speaking, this drag is considered negligible in relation to the drag on the catch. For a very small catch we suppose that this point is also debatable. Future work could verify this aspect.

The entrance diameter is constant and could be determined by the user in the present model. In a real trawl this point is questionable, and it would be more accurate to remove the constraint from this diameter. In this case, the twines emerge horizontally from the entrance contrary to Fig. 6.

The Newton–Raphson method has been used to solve the equilibrium of the cod-end, the Newmark scheme could also be used. The Newmark scheme does not use the Jacobian and is therefore easier to implement.

We suggest that these models of hexagonal mesh codends could be used in scientific studies: for example the theoretical investigation of codend performance, experimentally examined by Madsen et al. (2012) or Herrmann (2005), could be undertaken by combining the present models with the use of a codend size selection simulator like PRESEMO.

References

Alverson, D.L., Hughes, S.E., 1996. Bycatch: from emotion to effective natural resource management. Rev. Fish Biol. Fish. 6, 443–462.

Anon, 2005. EC Council Regulation No. 2187/2005, 21 December 2005. Technical Report. EC Council.

Herrmann, B., 2005. Effect of catch size and shape on the selectivity of diamond mesh cod-ends: I. Model development. Fish. Res. 71, 1–13.

Herrmann, B., Priour, D., Krag, L.A., 2006. Theoretical study of the effect of round straps on the selectivity in a diamond mesh cod-end. Fish. Res. 80, 148–157.

Herrmann, B., Priour, D., Krag, L.A., 2007. Simulation-based study of the combined effect on cod-end size selection of turning meshes by 90 and reducing the number of meshes in the circumference for round fish. Fish. Res. 84, 222–232.

Herrmann, B., Wienbeck, H., Moderhak, W., Stepputtis, D., Krag, L.A., 2013. The influence of twine thickness, twine number and netting orientation on codend selectivity. Fish. Res. 145, 22–36.

Madsen, N., Herrmann, B., Frandsen, R.P., Krag, L.A., 2012. Comparing selectivity of a standard and turned mesh t90 codend during towing and haul-back. Aquat. Living Resour. 25, 231–240.

O'Neill, F., 1997. Differential equations governing the geometry of a diamond mesh cod-end of a trawl net. J. Appl. Mech. 64, 7–14.

O'Neill, F., O'Donoghue, T., 1997. The fluid dynamic loading on catch and the geometry of trawl cod-ends. Proc. R. Soc. Lond. Ser. A: Math. Phys. Eng. Sci. 453, 1631–1648.

O'Neill, F., Priour, D., 2009. Comparison and validation of two models of netting deformation. J. Appl. Mech. 76.

Priour, D., 1999. Calculation of net shapes by the finite element method with triangular elements. Commun. Numer. Methods Eng. 15, 755–763.

Priour, D., 2003. Analysis of nets with hexagonal mesh using triangular elements. Int. J. Numer. Methods Eng. 56, 1721–1733.

Priour, D., 2013. A Finite Element Method for Netting: Application to Fish Cages and Fishing Gears, 1st ed. Springer.

Priour, D., Herrmann, B., O'Neill, F., 2009. Modelling axisymmetric cod-ends made of different mesh types. Proc. Inst. Mech. Eng. Part M: J. Eng. Maritime Environ. 223, 137–144.

Sistiaga, M., Herrmann, B., Nielsen, K.N., Larsen, R.B., Jech, J.M., 2011. Understanding limits to cod and haddock separation using size selectivity in a multispecies trawl fishery: an application of fishselect. Can. J. Fish. Aquat. Sci. 68, 927.

Wienbeck, H., Herrmann, B., Moderhak, W., Stepputtis, D., 2011. Effect of netting direction and number of meshes around on size selection in the codend for baltic cod (*Gadus morhua*). Fish. Res. 109, 80–88.